Tribology Letters (2022) 70:52
https://doi.org/10.1007/s11249-022-01594-3

ORIGINAL PAPER

Explore the Tribological Effects of Two N-Containing Functional Groups on O/W Emulsion

Yinglei Wu[1] · Emile van der Heide[2,3] · Zhongyi He[4] · Erik de Vries[2]

Received: 10 December 2021 / Accepted: 25 March 2022 / Published online: 16 April 2022

Abstract
Two water-soluble N-containing additives without sulfur and phosphorus, hexanamide with tetraethylenepentamine (EEHA) and benzotriazole amide with diethylenetriamine (BTAA), were synthesized and used as additives in the oil-in-water emulsion to investigate the effect of amino and benzotriazole ring on the tribological properties of the emulsion. The results showed that EEHA/BTAA exhibited wear resistance under all tested conditions. This may be attributed to the basic amino-functional groups in the additives which reduce the corrosive wear of the base emulsion. BTAA-emulsion showed the best friction-reducing and anti-wear performance under the 3 N loading condition, which may be attributed to its benzotriazole ring, which cannot be easily decomposed and could form self-assembled layers through π–π stacking. This π–π stacking may effectively compensate for the low chemical reactivity of the benzotriazole ring, and serve as a better protective film to exert tribological properties.

Keywords N-containing additives · Tribochemical mechanism · Self-assembled adsorption film · π–π stacking

1 Introduction

Friction and wear have an inevitable impact on metalwork, which usually leads to energy consumption and low equipment life [1, 2]. As a result, lubricants are very important to the machining of metals, and the correct use of lubricants can effectively extend the life of the machine and reduce the cost of metal processing. Meanwhile, continuous improvement of environmental awareness has prompted lubricant manufacturers to develop new lubricant formulations for metal processing, which have low friction and high anti-wear properties while meeting actual environmental requirements. Water-based lubricants had been used in many metal processing fields, such as metal cutting and metal forming, due to their outstanding characteristics of low cost, good environmental compatibility, and excellent flame resistance [3, 4].

As a widely used water-based lubricant, most oil-in-water (O/W) emulsions contain more than 80% water. Due to its high water content, O/W emulsion is suitable for hydraulic systems and metal processing equipment that require good cooling and flame retardant functions. The two main functions of O/W emulsion are particularly important to metalwork, which is to cool the friction surface and reduce friction and wear. Specifically, during metal processing, oil droplets can adsorb on the metal surface and form an oil film to lubricate the friction surface. Water can quickly take away friction heat from the friction zone for its high specific heat capacity to avoid metal adhesion and welding. Although O/W emulsions have many advantages over traditional oil-based lubricants [5], the presence of water also causes corrosion defects. To solve this problem, the best way is to develop additives suitable for O/W emulsions. The ideal performance is that it cannot only reduce metal corrosion but also reduce friction and wear.

In recent years, N-containing additives are expected to partially replace sulfur or phosphorus additives due to their corrosion resistance and environmental protection factors.

✉ Yinglei Wu
wuyl@sues.edu.cn

1 School of Chemistry and Chemical Engineering, Shanghai University of Engineering Science, Shanghai, China

2 Laboratory for Surface Technology and Tribology, Faculty of Engineering Technology, University of Twente, Enschede, The Netherlands

3 Soete Laboratory, Ghent University, Technologiepark Zwijnaarde 903, 9052 Zwijnaarde, Belgium

4 School of Materials Science and Engineering, East China Jiaotong University, Nanchang, China

A lot of research has been conducted on N-containing additives suitable for boundary lubrication. However, almost all the studies focus on oil-based systems. For example, Reddyhoff et al. [6] reported that adding octadecylamine $CH_3(CH_2)_{17}NH_2$ as a friction modifier to low viscosity fluids (such as cetane, low viscosity silicone oil, and toluene) can significantly reduce the boundary friction in micro-electromechanical systems (MEMS). González et al. [7] issued an amide-type ionic liquid, which can be used as a pure lubricant and a polar oil additive. Faujdar et al. [8] found that the amide N-phenyl-p-phenylenediamine-dodecenyl succinic anhydride can be used as a multifunctional and efficient lubricant additive for deposit control and lubrication.

Until now, almost all the research on O/W emulsions is concentrated on additives that are dissolved in oil droplets [9, 10]. As an important part of the O/W emulsion, the tribological effect of water is rarely studied, and the influence of additives in the water phase on tribological properties has not been reported. Based on the above background and problems, this study focused on the influence of aqueous phase change on the tribological properties of O/W emulsion to achieve synergy in the future with oil-soluble additives. For that, two water-soluble N-containing additives, EEHA and BTAA, without sulfur and phosphorus were synthesized. Both additives contain amino and amide functional groups as reported in the literature, and the number of nitrogen atoms was the same. The difference is that an additional benzotriazole ring was added to the molecular structure of the BTAA additive.

The design idea of the additives is as follows: There are two main explanations for the adsorption of additives on metal surfaces. One explanation is "solitary electron adsorption", that is, the polar end of the additive normally containing nitrogen or oxygen atom leads the molecule to be adsorbed on the metal surface. The possible reason is that the solitary electrons of the N atom can be coordinated with the empty d orbit of the metal atom, and can also be combined with the positive charge of the metal surface to form a stable complex adsorption film. Another explanation is the "π-electron adsorption" caused by nonpolar aromatic rings. It has been reported that some N-containing heterocyclic compounds, such as benzotriazole, benzimidazole, benzazole, thiazole, cyclotriphosphazene, and triazine derivatives have a compact structure and a high electronegativity (π-electron), which helps additives adsorb onto the metal surface to inhibit corrosion and to reduce wear [11]. In addition, there is a mutual attraction between aromatic molecules with π-electron conjugated structures, which is usually called the π–π stacking effect [12]. It is a non-covalent bond between aromatic systems. Therefore, it can theoretically lead to a small shear force between the accumulation layers. Therefore, is it possible to form an adsorption film, which can also be regarded as a self-assembled film through the adsorption and assembly of additive molecules on the metal surface as a low-shear lubricating film conducive to friction-reducing and anti-wear performance? However, aromatic structures such as benzotriazole generally show low reactivity. The first step for additive molecules to play a tribological role should be to adsorb on the metal surface, and then the tribochemical reaction occurs. Judging from the molecular structure, the tribological activities of the EEHA should belong to strong adsorption (multi-N) + more tribochemical activity ($–NH_2$), while BTAA should belong to strong adsorption (multi-N) + less tribochemical activity (benzotriazole ring). For nitrogen-containing additives, which is more favorable for tribological properties, adsorption film, or tribochemical reaction film? The present study attempts to elucidate the main points of the molecular design of nitrogen-containing additives by comparing the effects of nitrogen-containing molecular structure on tribological properties.

In short, two water-soluble N-containing additives were synthesized and used as additives for O/W emulsions. Additives change the composition of the water phase and should also cause changes in the tribological properties of the emulsion. Through the comparison of tribological properties, the influence of different forms of nitrogen-containing functional groups (amino and benzotriazole ring) on tribological properties can be explained from a molecular perspective. The interaction between oil droplets and water-based additives in the O/W emulsion system also can be revealed.

2 Materials and Methods

2.1 Synthesis of Additives

Figure 1 shows the synthetic routes of two amine additives and the appearance of the obtained products. The synthetic route of BTAA additive included 2 steps. Step 1, 40 g of benzotriazole, 150 mL of deionized water, and 16.0 g of NaOH were added to a 500 mL three-necked flask, and then 36 g of the chloroacetic acid aqueous solution was added dropwise to the reaction mixture within 30 min, and the reactants were stirred at 90℃ for 3 h. After the reaction was completed and cooled to room temperature, hydrochloric acid was added to the product until a large number of white precipitates appeared. Subsequently, the product was filtered and washed with deionized water 3 times and then dried under vacuum to obtain the intermediate product 2-(1-benzotriazolyl) acetic acid. Step 2, diethylenetriamine was added into a 500 mL three-necked flask and kept stirring, then benzotriazole acetic acid intermediate product was slowly added dropwise to diethylenetriamine according to the 1:1 molar ratio. An appropriate amount of xylene was also added as a solvent and water-carrying agent. The

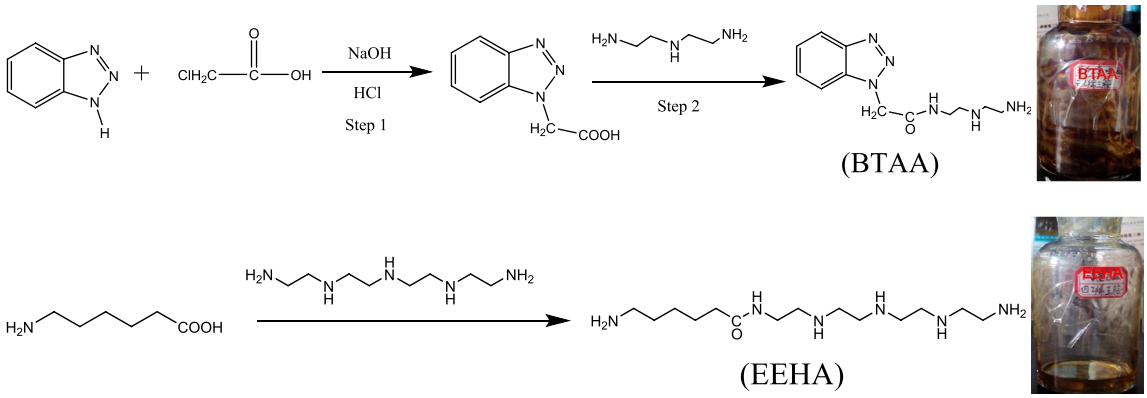

Fig. 1 Synthetic route and product appearance of two amine additives

Table 1 Basic information of the two additives

Additive	Molecular formula	Molecular weight (g/mol)	N% (weight)
EEHA	$C_{14}H_{34}N_6O$	302.47	27.79
BTAA	$C_{12}H_{18}N_6O$	262.32	32.04

mixed reactants were subjected to an amidation reaction at 140℃ for about 6 h until no water was formed. The purification of the synthesized monoamide was carried out with silica gel as a stationary phase and a mixed solution of volume (1,2-dichloroethane): volume (acetic acid) = 6:1 as the mobile phase for column separation. In the purification process, TLC was used to analyze the purity. Finally, after the vacuum distillation step a yellow–brown viscous liquid N-(2-((2-aminoethyl)amino)ethyl)-2-(1H-benzo[d][1,2,3] triazol-1-yl) acetamide was obtained, and coded as BTAA.

The synthesis of EEHA was relatively simple: 6-aminocaproic acid was dropwise added to the stirred tetraethylenepentamine at a molar ratio of 1:1. Xylene was used as a solvent and water-carrying agent, and the three-necked flask was equipped with a thermometer, a water separator, a stirring rod, and a reflux condenser. The acylation dehydration section was maintained at 130 °C for about 6 h until no water was distilled out. The initial product obtained by the reaction was subjected to purification and vacuum distillation according to the methods used for BTAA to obtain the final product 6-amino-N-(2-((2-((2-((2-aminoethyl)amino)ethyl) amino) ethyl)amino)ethyl) hexanamide, which showed a light yellow sticky appearance and was coded as EEHA in this article.

2.2 Material Characterization

Table 1 gives basic information about the two synthesized compounds, EEHA and BTAA. The novel products were characterized utilizing infrared spectroscopy (FTIR), nuclear magnetic resonance spectroscopy (NMR, ^{1}H, and ^{13}C), and elemental analysis.

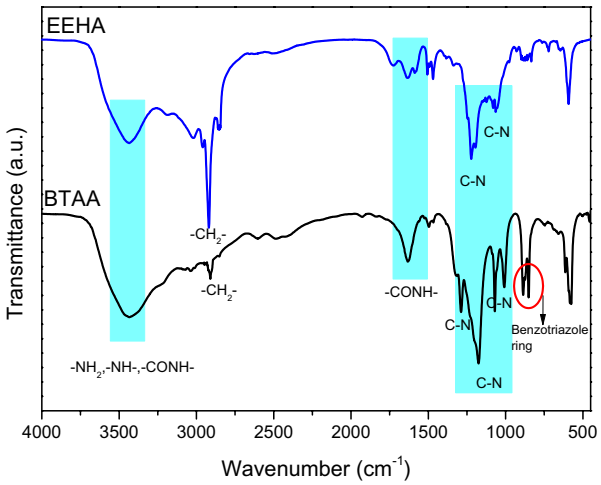

Fig. 2 FTIR spectra of EEHA and BTAA additives

FTIR spectra were obtained by a Paragon 1000 FTIR spectrometer (PerkinElmer). ^{1}H and ^{13}C NMR spectra were measured using a Bruker AV 600 NMR spectrometer (Bruker, Germany), and tetramethylsilane was used as the internal standard. The C, H, N elemental analysis of the synthesized additives was performed on a Perkin-Elmer 2400CHN elemental analyzer.

2.2.1 FTIR

Figure 2 displays the FTIR spectra of EEHA and BTAA additives. New absorption peaks around 3430 cm^{-1} were both observed in spectra EEHA and BTAA, which should be corresponded to the N–H stretching vibration in the amino group (–NH_2, –NH–, –CONH–). The band at 1630 cm^{-1} provides evidence of the formation of amide

linkage (–CONH–). Peak around 2900 cm^{-1} in two spectra can chiefly correspond to methylene (–CH_2–). The other typical peaks that appeared at 884.63 and 848.4 cm^{-1} were attributed to the benzotriazole ring in BTAA. These peaks indicated the presence of an aromatic nucleus in the BTAA additive, while they didn't appear in the additive of EEHA. Absorption peaks at 1283.99, 1171.89, 1069.4, and 1005.34 cm^{-1} represent C–N in BTAA, including in-plane asymmetric stretching vibration of benzotriazole. And for the EEHA additive, the C–N bond can be verified from the absorption peaks at 1219.93 and 1056.58 cm^{-1}.

2.2.2 NMR

The assignments of ^{1}H NMR for EEHA compound (DMSO, internal standard: TMS, δ (ppm)) are: 1.28–1.35 (m, –C**H$_2$**–C**H$_2$**–CH_2–C(O)–); 1.51 (m, –N**H$_2$**, –CH_2–N**H**–CH_2–); 1.52 (m, –C**H$_2$**–$(CH_2)_3$–C(O)–); 2.13 (t, –C**H$_2$**–C(O)–); 2.53 (m, –CH_2–NH–(C**H$_2$**)$_2$–NH–(C**H$_2$**)$_2$–NH–); 2.62 (m, –NH–CH_2–C**H$_2$**–NH_2); 2.66 (m, –NH–C**H$_2$**–CH_2–NH_2, –C(O)–NH–CH_2–C**H$_2$**–NH–); 2.69 (m, NH_2–C**H$_2$**–$(CH_2)_4$–C(O)–); 3.53 (m, –C(O)–NH–C**H$_2$**–); 8.02 (m, –C(O)–N**H**–).

^{1}H NMR for BTAA compound (DMSO, internal standard: TMS, δ (ppm)) are: 1.51 (m, N**H$_2$**–$(CH_2)_2$–N**H**–); 2.63–2.68 (m, NH_2–CH_2–C**H$_2$**–NH–C**H$_2$**–); 3.52 (m, NH_2–$(CH_2)_2$–NH–CH_2–C**H$_2$**–); 5.62 (s, –C**H$_2$**–C(O)–); 7.35–7.84, 8.07 (m, **H** in benzotriazole); 8.02 (t, –C(O)–N**H**–).

The assignments of ^{13}C NMR for EEHA compound (DMSO, internal standard: TMS, δ (ppm)) are: 25.2–27.4 (–C(O)–CH_2–(**C**H_2)$_3$–); 36.6 (–C(O)–**C**H_2–); 39.5 (–C(O)–NH–**C**H_2–); 41.1–42.2 (NH_2–**C**H_2–); 48.5–49.1 (–**C**H_2–NH–**C**H_2–**C**H_2–NH–); 51.3 (NH_2–CH_2–**C**H_2–NH–); 177.6 (–**C**(O)–).

^{13}C NMR for BTAA compound (DMSO, internal standard: TMS, δ (ppm)) are: 39.2 (–C(O)–NH–**C**H_2-); 41.1 (NH_2–**C**H_2–); 48.5 (–C(O)–NH–CH_2–**C**H_2–); 51.3 (NH_2–CH_2–**C**H_2–); 61.7 (–**C**H_2–C(O)–); 110, 119.5, 126.3, 132.9, 145.6 (**C** in benzotriazole); 166.5 (–**C**(O)–).

The NMR spectra (^{1}H, ^{13}C) of EEHA and BTAA confirm that the as-prepared N-containing compounds were the targeted products, each peak corresponds to the related chemical structure.

2.2.3 Elemental Analysis

The synthesized products were also characterized by a method of elemental analysis. The results of elemental analysis are listed in Table 2. It can be seen that the obtained results are in good agreement with the target compounds within the experimental error of lubricant additives.

Table 2 Elemental analysis data of the additives (Found/calculated, wt%)

Items	C	H	N
EEHA	55.48/55.59[a]	11.21/11.33[a]	27.82/27.79[a]
BTAA	54.88/54.95[a]	6.95/6.92[a]	32.13/32.04[a]

[a]Calculated value (oxygen being at balance)

Table 3 Typical properties of rapeseed oil

Item	Value
Density (20℃), g/cm^3	0.92
Viscosity, mm^2/s	
40 ℃	31.3
100 ℃	8.3
Viscosity index	217
Flash point (open cup)	330 ℃
Acid value (KOH)/(mg/g)	≤4.0

2.3 Emulsions Preparation

As an environmentally friendly lubricant, rapeseed oil not only possesses good lubricating properties and high-biodegradability but also renewable resources. In addition, Hsien stated that canola oil (rapeseed oil) is one of the most suitable base oil for the formation of metalworking fluids [13]. Therefore, in this study, rapeseed oil from Xi'an Jiali Oil and Grease Factory of China was used as the base oil for preparing O/W emulsion without any further treatment. In common oilseed crops, the most abundant is oleic acid, a monounsaturated fatty acid with a chain of 18 carbon atoms. The other typical properties of used rapeseed oil are shown in Table 3.

In the preparation of emulsions, the nonionic surfactant, polyoxyethylene 20-sorbitan monooleate (polysorbate 80/Tween 80) supplied from Sigma-Aldrich was added as an emulsifier to deionized water and stirred by a magnetic stirrer operated at 800 rpm for 10 min to obtain a premix. Next, rapeseed oil was added to the premix to obtain base emulsion, assisting with 30 min stirring. Then, the additive was mixed into the base emulsion and stirred for 30 min to prepare the additive-containing emulsion. Before obtaining the final experimental samples, 30 min of homogenization operation by the apparatus of Ultra Turrax T25 was also implemented. The composition of each experimental sample prepared was 6 wt% rapeseed oil, 4 wt% emulsifier, and 0.5 wt% additive. The viscosity of the obtained emulsions is about 1.53×10^{-3} Pa s.

2.4 Friction Test

The tribological properties of the additive were studied using a ball-on-ring friction meter (CSM instrument), Fig. 3 shows the photo and schematic diagram. 52,100 bearing steel balls (diameter 10 mm) and steel rings were used as friction pairs. The ring was fixed by matching accessories, so the overall effect was equivalent to a pin-on-disk model. Before each test, the rings and balls shall be cleaned with acetone and isopropanol and dried for standby. The surface roughness (Ra) of the balls and rings before the tests was obtained by a keyencevk9700 laser scanning microscope. All friction tests were repeated at least three times at room temperature (~20℃) to ensure repeatability. Table 4 lists the friction conditions in this study. The contact pressure can be calculated according to the Hertzian equation of point contact.

For the estimation of the lubrication regime, various theoretical models have been proposed, including the representative Hamrock and Dowson (later revised by Esfahanian and Hamrock) [14]. In their model, the Λ plays an important role, and the friction mechanism is further related to this information. Determination of speed and pressure is based on the theory outlined in reference [14] to ensure that the initial lubrication state is boundary lubrication ($\Lambda \leq 1$), thereby distinguishing the tribological properties of two additives on the boundary lubrication film.

2.5 Worn Surface Analysis

Before various examinations after the friction test, the steel balls and rings need to be cleaned with acetone and isopropanol to obtain clean worn surfaces. To scrutinize the wear mechanism of the tribologically stressed surfaces, the wear tracks were investigated through 3D wear spot morphology scanning, chemical composition identification, and nanomechanical assessment of tribofilms. The surface topographies of the balls were observed with a 3D laser scanning confocal microscope. Wear tracks of the rings were examined by a Micromap 560 white light interferometer from Micromap corp (Tucson, AZ, USA).

Table 4 Friction test conditions

Parameters	Value
Load	1 N, 2 N, 3 N
Sliding velocity	60 mm/s, 120 mm/s
Sliding distance	100 m
Ball diameter	10 mm
Roughness (Ra)	Ball: 30 ± 10 nm Ring: 100 ± 50 nm

Since the tribochemical reactions during the friction process are extraordinarily perplexing and cannot be detected in situ up to date, surface analysis after the rubbing process is an effective method to figure out the reason for different friction-reducing and anti-wear performance. In this work, semi-quantitative component analysis of worn surface was performed using an energy dispersive X-ray spectrometer (EDS, Phenom prox) equipped with SEM. Raman spectra analysis was carried out to investigate the surface structure after the friction test, using a Raman spectrometer (Senterra R200-L) with a laser source of 532 nm. X-ray photoelectron spectroscope (XPS) and X-ray absorption near-edge structure (XANES) spectroscopy were also employed to identify the chemical state of tribofilms after the friction tests. XANES analysis was performed at Beijing Synchrotron Radiation Facility.

The nanoscale mechanical properties of the tribofilms on the rings were measured by nanoindentation. Details of the instrumentation and calibration have been given in our previous research [15]. Nanoindentation experiments were performed using a 25 μN load, which can make the influence of the underlying substrate negligible. To estimate the experimental error, three indentations were performed. To randomize the test points, nanoindentation alternately appeared on the positions inside and outside the wear trajectory.

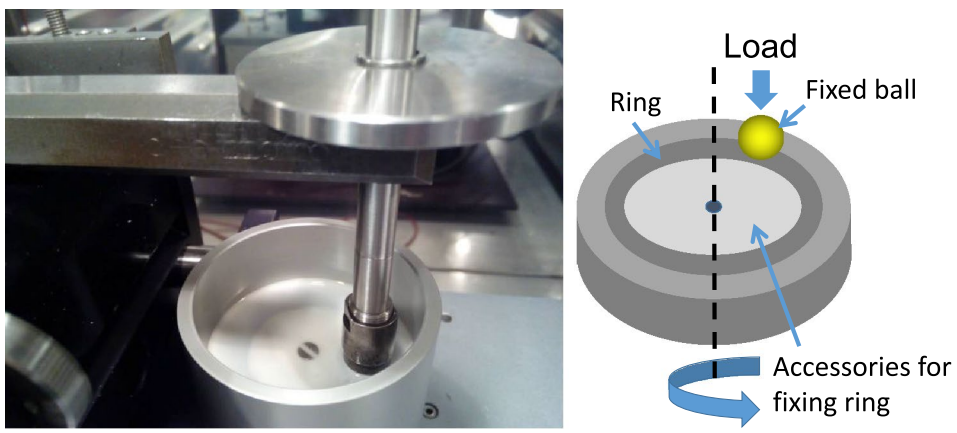

Fig. 3 Photo and schematic diagram of a ball-on-ring setup for the tribological test

3 Experimental Results

3.1 Friction-Reducing Performance

Figure 4 shows the friction-reducing performance of the three emulsions under a constant load of 1 N at two different sliding velocities 60 mm/s and 120 mm/s. It can be seen that the coefficient of friction (COF) of the emulsion containing amide additive is increased in comparison with the base emulsion, indicating that the additive affects the "plate-out" [16] of the emulsion droplets. More specifically, the additives may adsorb faster than the emulsion droplets onto the metal surface. This can be explained as follows: Once the metal surfaces were exposed to the emulsion, the formation of a multilayer molecular adsorption film begins. The polarity of additive allows it to be adsorbed on the surface of the steel ball, competing with the adsorption of rapeseed oil. The polarity of the additive might be greater than that of rapeseed oil and surfactant Tween 80 so that almost every available metal surface site can be quickly occupied by additive molecules and eventually lead to failure of "plate-out" of the oil film, and hence cause increased COF. It can also be seen from Fig. 4 that the friction-reducing performance of BTAA is better than that of EEHA. This may be attributed to the difference in molecular structure. Combined with the subsequent analysis of wear resistance and worn surface, the molecular mechanism of both can be analyzed more clearly. From Fig. 4 it can also be informed that for the three emulsions studied at the two set sliding speeds, the COF at a high speed of 120 mm/s was reduced compared to that of 60 mm/s, which is consistent with our earlier research, that is, under the same working conditions, the higher the friction velocity, the more likely the system will transition from a boundary regime to a mixed lubrication regime, and vice-versa.

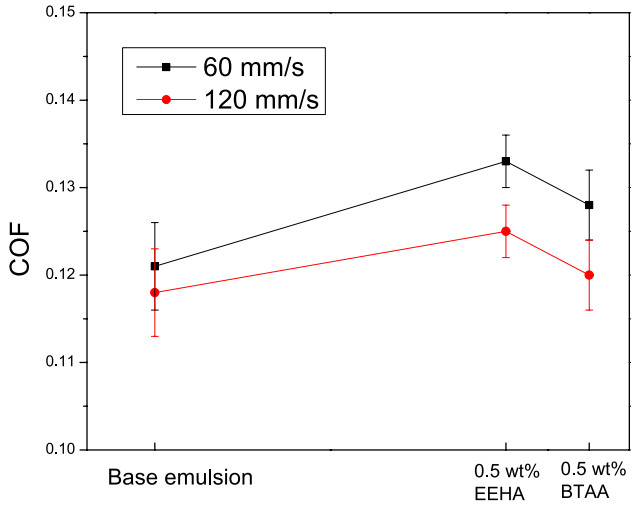

Fig. 4 The effect of friction velocity on COF for three different emulsions (load 1 N)

The effect of load on the COF was also investigated and the results are shown in Fig. 5a. For base emulsion lubrication, the COF increases with the increase of contact pressure. While the COF corresponding to BTAA-emulsion lubrication shows the opposite trend to that of the base emulsion. Under 1 N loading condition, the COF in the case of base emulsion is less than those of EEHA- and BTAA-emulsion. The possible reason could be that because of the "plate-out" effect, oil molecules can form a better adsorption film than EEHA and BTAA molecules under low load, thereby reducing COF. More specifically, the polar groups of the oil molecules, such as the carboxyl of fatty acid were strongly attracted to the metallic surface. The non-polar tails, which were alkyl groups formed the molecular brush. The

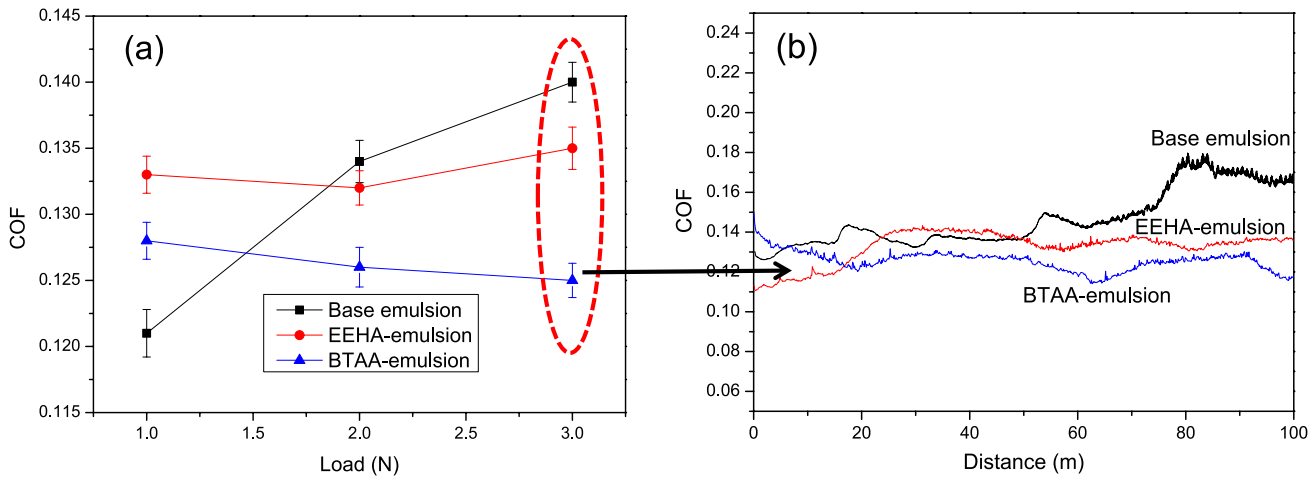

Fig. 5 The effect of load on COF for three different emulsions (velocity 60 mm/s)

repulsion or weak bonds between the contacting alkyl groups led to the relatively low-sshear strength of the rubbing interface. However, under high loads of 2 N and 3 N, the corresponding COFs of the three emulsions can be ranked: base emulsion > EEHA-emulsion > BTAA-emulsion. This indicates that the adsorption film formed by rapeseed oil can be easily destroyed, and it cannot form an effective tribochemical reaction film as additive molecules did, thus leading to a higher COF. The experimental results suggest that the increase in load is beneficial for EEHA and BTAA to form a more effective friction film on the friction surface. The possible reason is that on the one hand, due to the high nitrogen content, the additive molecules can be closely adsorbed on the metal surface and are not easy to remove. On the other hand, high load friction will accumulate more frictional heat to trigger the tribochemical reaction. In addition, the tribofilm formed by BTAA-emulsion under high load was more effective than that formed by EEHA-emulsion, which should be attributed to the benzotriazole ring in the BTAA molecule. Its action mechanism during the friction process can be analyzed to a certain extent from the dynamic change curve of the COF.

During the process of sliding, heat will be generated between the rubbing surfaces due to the frictional contact of the tribopair. According to the basic theory of tribology, the macroscopic tribopair surface shows many irregular asperities under a microscope. Therefore, the actual contact area is only a small part of the surface of the tribopair, and the locally elevated temperature due to friction is referred to as the "flash temperature" [17]. So far, various models [18] have been developed to calculate this friction-induced flash temperature. According to Archard's law [19], the flash temperature is directly proportional to the frictional speed and load, and inversely proportional to the thermal conductivity of the friction pair. However, the local high flash temperature does not mean that the temperature of the overall frictional interface is high as well, for the following three reasons: (1) Local high temperatures typically last only a few milliseconds, and once these contact peaks disengage, the temperature drops rapidly [20]. (2) The friction material used in this study is steel, which has good thermal conductivity [21]. (3) The emulsion used contains about 90% water. Water has a high specific heat capacity (4.2×10^3 J kg^{-1} $℃^{-1}$) and thus could take the friction heat away quickly during the sliding process. Since the tests of this study were carried out at room temperature, it can be speculated that the local friction heat generated during the friction process can be quickly dissipated for the above-mentioned reasons. However, the high flash temperature created at the moment of asperities' engagement could induce the tribochemical reaction between the additive and the metal surface and form various tribofilms. Therefore, it can be considered that the plastic deformation of the steel tribopair caused by frictional heat is negligible, and the difference in the tribological properties of different lubricants can be attributed to the different tribofilms formed. The formation of tribofilms with different tribological properties should be ascribed to the differences in the molecular structure and chemical properties of the additives.

Friction evolutions along distance under 3 N loading conditions are shown in Fig. 5b. It is worth noting that the EEHA-emulsion shows the smallest initial but rising COF in the sliding distance of the first 20 m. The situation of BTAA-emulsion is the opposite. Although the initial COF is relatively large, it shows a declining trend. This may be because almost all EEHA molecules were in the water phase and can quickly adsorb to the metal surface. However, because BTAA contains hydrophobic benzotriazole ring, it is speculated that some BTAA molecules play the role of surfactant and were located at the water–oil interface, so their adsorption speed to the metal surface is slower than that of most EEHA molecules dissolved in water. The declining trend of COF corresponding to BTAA-emulsion lubrication also means that the tribofilm formed by BTAA molecules was not easily damaged and may become more and more effective. In terms of the steady-state between 20 and 50 m, COFs of base and EEHA-emulsion approach a similar value about 0.135. Nevertheless, the overall friction evolution is better in EEHA-emulsion than that in the base emulsion, in terms of consistently smooth frictional evolution with less standard deviation. COF of base emulsion increased with friction continued, which could be attributed to the failure of tribofilm. The COF curve corresponding to BTAA-emulsion in Fig. 5b shows the smallest value in the steady-state, illustrating that the tribofilm generated by BTAA molecules was the most durable and cannot easily be removed.

3.2 Anti-wear Properties

The wear scars of the ball were inspected and wear rates at various conditions were calculated as the method in reference [22]. As shown in Fig. 6, it can be seen that compared with the effect of base emulsion, the N-containing additive reduced the wear rate of the steel ball under all tested conditions, indicating the anti-wear effect of the additives used. This may be attributed to the basic amino-functional groups contained in the synthesized additives, which can effectively reduce the corrosion wear of the metal surface. Furthermore, under 1 N loading condition, the anti-wear property of EEHA additive is greater than that of BTAA additive, indicating that EEHA additive can form a more effective anti-wear tribofilm on the metal surface. This may be due to the following two reasons: (1) EEHA possesses a longer chain length and more amino groups than BTAA molecules, which means that under low loading, EEHA molecules are probably vertically adsorbed on the metal surface, and may form a thicker adsorption film together with

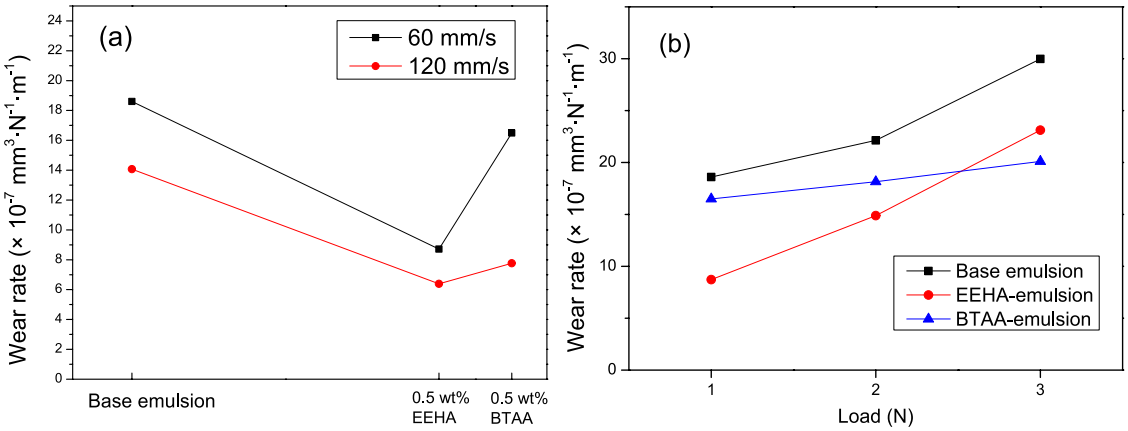

Fig. 6 The anti-wear properties for the three emulsions under different conditions **a** load 1 N, **b** velocity 60 mm/s

water molecules through hydrogen bonds. (2) Compared with the benzotriazole group in the BTAA molecule, the chemical bond in EEHA is easier to break, and the 1 N load is enough to cause more tribochemical reactions between EEHA and metal surface to form a tribofilm with an anti-wear effect.

Interestingly, comparing the wear rates corresponding to EEHA- and BTAA-emulsion, it can be found that although the wear rates of EEHA-emulsion under 1 N and 2 N loads are lower, the wear rate under 3 N load is higher than that of BTAA-emulsion. This means that heavy load might be more conducive to BTAA's anti-wear performance. The possible reason could be: (1) High loading can reduce the distance between aromatic rings and enhance the conjugation of π electrons. Therefore, the benzotriazole rings can form more regular π–π stacks under the condition of 3 N loading, while the possibility of dislocation pile-up under light loading is greater. For EEHA-emulsion lubrication, low loading is more conducive to the vertical adsorption of linear EEHA molecules on the metal surface to form thicker molecular brushes. (2) EEHA is more prone to tribochemical reaction with the steel surface than BTAA. The accumulated frictional heat under the load of 1 N or 2 N is enough to cause the tribochemical reaction of EEHA to form a tribofilm on the rubbing surface. However, based on Archard's law [19], higher flash temperature (greater frictional heat) can be generated by friction under a higher load of 3 N, which means 3 N load condition may trigger a faster tribochemical reaction between BTAA and the metal surfaces. In short, the 3 N load condition should be related to the high-quality or fast formation of BTAA-tribofilm.

3.3 Worn Surface Analysis

3.3.1 Morphologies and Nanomechanical Evaluation

Figure 7 displays the morphologies of the wear scars on balls and rings after wear tests under 3 N loading conditions with three different emulsions, as well as nanoindentation results of the tribofilms on rings. Among the three, the wear scars (Fig. 7a1, a2) corresponding to base emulsion lubrication show the largest size. There are many deep and wide furrows, as well as obvious rust spots on the surface of the wear scars. This characterizes the action of a micro-cutting mechanism on the hard steel surface. However, it is observed that for BTAA-emulsion, the surface of the wear scar is smoothest, the wear scar and the rust condition are slightest (Fig. 7c1, c2). Compared with the results of BTAA-emulsion, the wear scar after lubrication of EEHA-emulsion is relatively larger, and the roughness of the corresponding worn track on the ring is also greater. Figure 7 confirms that BTAA can effectively reduce the wear of friction pairs under 3 N loading. It can be inferred that the BTAA additive can form a protective film on the rubbing surfaces. On the one hand, the protective film might effectively prevent the rubbing surfaces from direct contact with each other, thus reducing wear. On the other hand, BTAA-tribofilm played a role in corrosion inhibition and provided effective physical isolation between the masked substrate and the corrosive medium of water. This can be confirmed from the rust images of the worn scars on the balls.

The 3D morphologies of wear tracks on rings in Fig. 7a2, b2, c2 also give roughness information after rubbing with different lubricants: base emulsion (Sq: 834.5 nm, Sa: 670.3 nm), EEHA-emulsion (Sq: 763.1 nm, Sa: 602.2 nm), and BTAA-emulsion (Sq: 762.3 nm, Sa: 542.0 nm). Hence, it can be inferred that the BTAA-emulsion has performed better than the base and EEHA-emulsion in preventing the tribopair contact and wear under the 3 N friction condition.

Figure 7a3, b3, c3 shows the representative nanoindentation force versus depth curves (F-D curve) from experiments performed on the wear track with an indentation load of 25 μN. The non-friction areas off the tracks were also examined for comparison. Due to the change of selected test points,

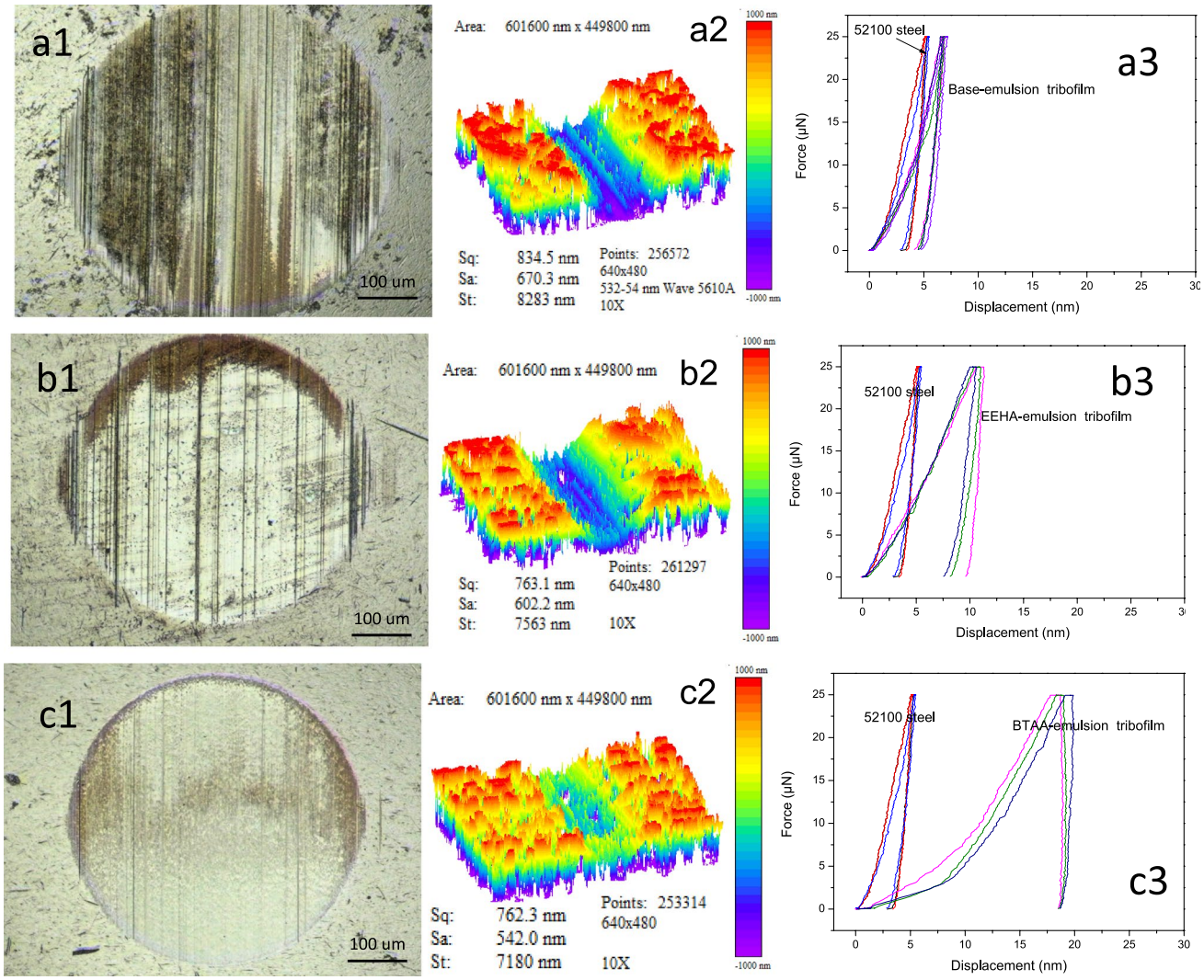

Fig. 7 Wear morphology of the balls (a1, a2, a3), rings (b1, b2, b3), and the nanoindentation of the tribofilms on the rings (c1, c2, c3) after lubricating with base emulsion (**a**), EEHA-emulsion (**b**) and BTAA-emulsion (**c**), respectively. (velocity 60 mm/s, load 3 N)

the loading part of the curve is slightly different, but the deviation of the results of multiple tests was small. By following the Oliver and Pharr method [23], it can be seen from the F-D curves that the elastic behaviors of the on and off wear track surfaces were significantly different. The F-D curves corresponding to the unrubbed areas show steeper slopes than that obtained on wear tracks, indicating that the steel matrix is stiffer than tribofilms. Nanoindentation results indicate that, for a given indentation force, the wear track surface exhibited more plastic deformation than the untested surface. This should be attributed to the presence of a tribofilm on the wear track. The F-D curves imply that the three formed tribofilms are softer than the steel substrate, and BTAA-tribofilm showed the most prominent softness. The above nanomechanical results reveal that the EEHA- and BTAA-tribofilm behaved as soft layers on the steel substrate.

3.3.2 Raman

Raman measurements of the as-obtained worn surfaces were carried out, as illustrated in Fig. 8. It can be seen that all Raman spectra can observe absorption peaks in the range of 400–700^{-1}, which should be ascribed to the metal–oxygen lattice vibrations [24], suggesting the presence of iron oxide. From the Raman spectrum corresponding to BTAA-tribofilm, it can be found that there is a ring deformation mode [25] at 786 cm^{-1}, and a ring breathing characteristic at 1100 cm^{-1}. The band at 1100 cm^{-1} involves C-H bending in the benzotriazole ring, N–H amine bending and C–N azo stretching [26]. The peak at 1350 cm^{-1} represents the stretching of the triazole ring; the peak at 1598 cm^{-1} could be the stretching of the benzene ring [27]. It can be inferred that there were

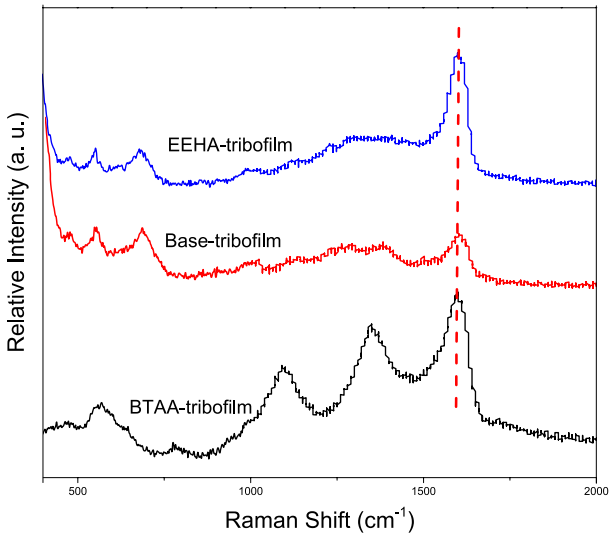

Fig. 8 The Raman spectra of the worn surface lubricated with different emulsions (velocity 60 mm/s, load 3 N)

substances containing benzotriazole ring structure on the surface of BTAA-tribofilm. In comparison with the bands corresponding to BTAA-tribofilm, only a band at around 1598 cm^{-1} is observed in the spectra of base-tribofilm and EEHA-tribofilm, which is the fingerprint frequency region for most organic molecules. Raman spectra confirm the existence of benzotriazole rings in the BTAA-tribofilm.

3.3.3 EDS

In order to better analyze the formation possibility of self-assembled aggregates, the surface composition of BTAA-tribofilm after friction was analyzed by EDS. Figure 9a and b show confocal images of the original unworn ring surface and wear track after rubbing with BTAA-emulsion, respectively. Figure 9c–f shows the EDS image and the spectra of the worn surface obtained from inside the wear track in Fig. 9b. EDS spectra show the presence of Fe and Cr inside the wear track. Fe and Cr come from the underlying matrix and so could be used as a semi-quantitative measure of the tribofilm thickness. The higher the Fe and Cr levels, the lower the tribofilm thickness. This method has been widely used to provide thickness and wear resistance of the tribofilm [28, 29]. Three analysis points were selected from the worn surface in Fig. 9c. Point 1 is the agglomerates located in the deep part of the furrow, point 2 is the agglomerates in the shallow part of the wear scar, and point 3 is the exposed part without obvious residue on the wear scar. Figure 9d–f shows the point component analysis of the agglomerates that BTAA may self-assemble during the friction process.

Many grooves can be seen on the surface of Fig. 9c. The grooves consistent with the friction direction were caused

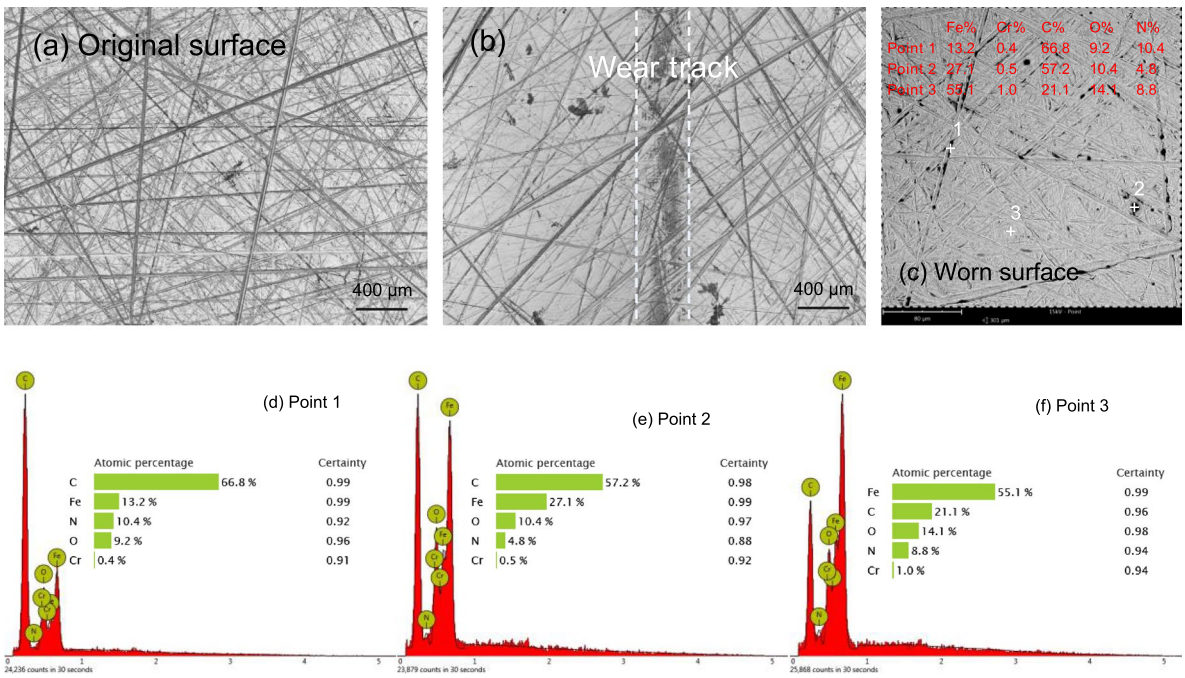

Fig. 9 **a** Confocal image of original ring surface; **b** Confocal image of wear track after rubbing with BTAA-emulsion; **c** EDS image of the worn surface in wear track; and **d–f** Point component analysis of the agglomerates formed by the possible self-assembly of BTAA during the friction process (velocity 60 mm/s, load 3 N)

by the scratch of the asperities on the tribopair, and deeper grooves related to higher loads. The grooves inconsistent with the friction direction were the original roughness of the steel ring used, and the inside pile-up substances were mainly caused by the accumulation of removed tribofilms. It can be seen in Fig. 9c–f that the carbon content at point 1 is the highest, followed by point 2, and the lowest at point 3. For iron content, the order is exactly the opposite, showing point 3 > point 2 > point 1. This indicates that the sediments are high-carbon substances, and the carbon content in the deep furrow is higher than the carbon content in the shallow furrow. Observing the molecular structure of BTAA, it can be found that the carbon atoms are mainly concentrated in the benzotriazole ring structure.

If the point to be measured was in a groove caused by scratches, EDS results indicate that the increase in load may destroy BTAA molecules and accumulate more carbonaceous substances. The increase in load can also shorten the distance of π electron clouds between adjacent molecules, thus increasing the tendency to form π–π conjugated accumulations. Based on the molecular structure of BTAA, it can be inferred that the aggregates could be π–π deposits. If the measured point was located in the groove caused by the roughness, EDS results indicate that the removed BTAA-tribofilm were trapped by the grooves on the rough surface, and the main component is a high-carbon-containing substance. Since the forming and removing of the tribofilms is a dynamic process, this implies that the BTAA-tribofilm is a high-carbon substance formed by destroyed BTAA molecules. Based on the above two analyses, it can be speculated that BTAA molecules were sheared and damaged during friction, and the formed friction film was likely to be formed by π–π stacking of benzotriazole rings.

3.3.4 XPS

The chemical compositions of worn surfaces lubricated with base, EEHA- and BTAA-emulsions were analyzed by XPS to further explore the friction mechanism. Figure 10 displays XPS wide scan and XPS spectra of N_{1s}, C_{1s}, O_{1s}, and Fe_{2p} on the worn steel surfaces lubricated by three different emulsions. The corresponding substance of each separated peak was queried from the NIST XPS Database [30]. As can be seen from XPS wide scan spectra, peaks appearing at around 400 eV, 286 eV, 531 eV, and 710 eV correspond to N_{1s}, C_{1s}, O_{1s}, and Fe_{2p}, respectively. C, O, and Fe elements can all be found on examined worn surfaces, whereas N was only detected on EEHA- and BTAA-tribofilm. This is consistent with expectations because nitrogen originates from additives, while there is no nitrogen in the base emulsion.

The N_{1s} spectra for the worn steel surfaces lubricated with EEHA- and BTAA-lubricant systems all exhibit an XPS peak around 400 eV, indicating that the N element in the two additives still exists in an organic state after sliding for 100 m. In addition, the four fitting peaks of N_{1s} spectra in EEHA-tribofilm correspond to –CONH– (400.1 eV), C–N (399.87 eV), $–NO_2$ (`399.4 eV), and –NH– (398.7 eV), respectively. An additional N = N (400.4 eV) peak appears in BTAA-tribofilm, which should be attributed to the benzotriazole ring in the BTAA additive, or generated compounds containing N = N bond. The N_{1s} spectra indicate that possible N-containing species on the worn surface were the undecomposed additive or its decomposed products such as organic amide, nitrile, azo compounds, or N-containing polymer [31].

The XPS C_{1s} spectra in Fig. 10 show fitting peaks that relate to various bonding states of carbon atoms. The C_{1s} peaks at 286, 284.8, and 284.3 eV correspond to C=O, C–C, and -COOH bonds in tribofilm resulting from the base emulsion, indicating that the rapeseed oil was adsorbed on the rubbing surfaces and may be oxidized during the friction process. For EEHA-tribofilm, the C_{1s} peaks at 286 and 284.8 eV are assigned to the C=O and C–C bonds, respectively. This indicates that the –COOH group produced by the EEHA additive was relatively small, most EEHA molecules were not oxidized. For BTAA-tribofilm, C_{1s} spectra were deconvoluted into three peaks including 288.7, 286, and 284.8 eV, which are, respectively, assigned to C–N, C = O, and C–C. The most obvious difference between the C_{1s} spectra of BTAA-tribofilm and EEHA-tribofilm is the appearance of the C–N peak, which shows that the damage of BTAA molecules during the friction process was smaller than that of EEHA, and the C–N bond is not completely cleaved.

The O_{1s} peaks for base-tribofilm confirm the existence of –CO– and –OH, which should be ascribed to the composition of rapeseed oil. This indicates that rapeseed oil had at least adsorbed on the rubbing surfaces. Additionally, O_{1s} spectra confirm that the oxidation reaction had occurred on the friction surface of steel and generated iron oxides, mainly Fe_2O_3. For additive-containing lubrication, the O_{1s} XPS peaks show that EEHA- and BTAA-tribofilms both contain nitrogen oxides, and special aromatic compounds appear in BTAA-tribofilm. Detailed analysis by comparing the fitting area of Fe_2O_3 in O_{1s} spectra indicates that the N-containing additives possess the effect of corrosion resistance, leading to the oxidation of iron taking place preferentially on the components without additives. This result agrees well with the corrosion status of surfaces shown in Fig. 7.

The Fe_{2p} peaks appearing at 713.7 eV correspond to 2p3/2 of zero-valent iron, which is the substrate of the friction pairs. The peak in Fe_{2p} at 711.2–711.4 eV corresponds to Fe_xO_y, which is consistent with the results of O_{1s} binding energy at 529.6–529.8 eV. Combining the $Fe_{2p3/2}$ peaks at 710 eV corresponding to Fe(NO)CH– for EEHA-tribofilm, and 710.1 eV corresponding to $[Fe(C_4H_2NCC_6H_5)_4]$- for

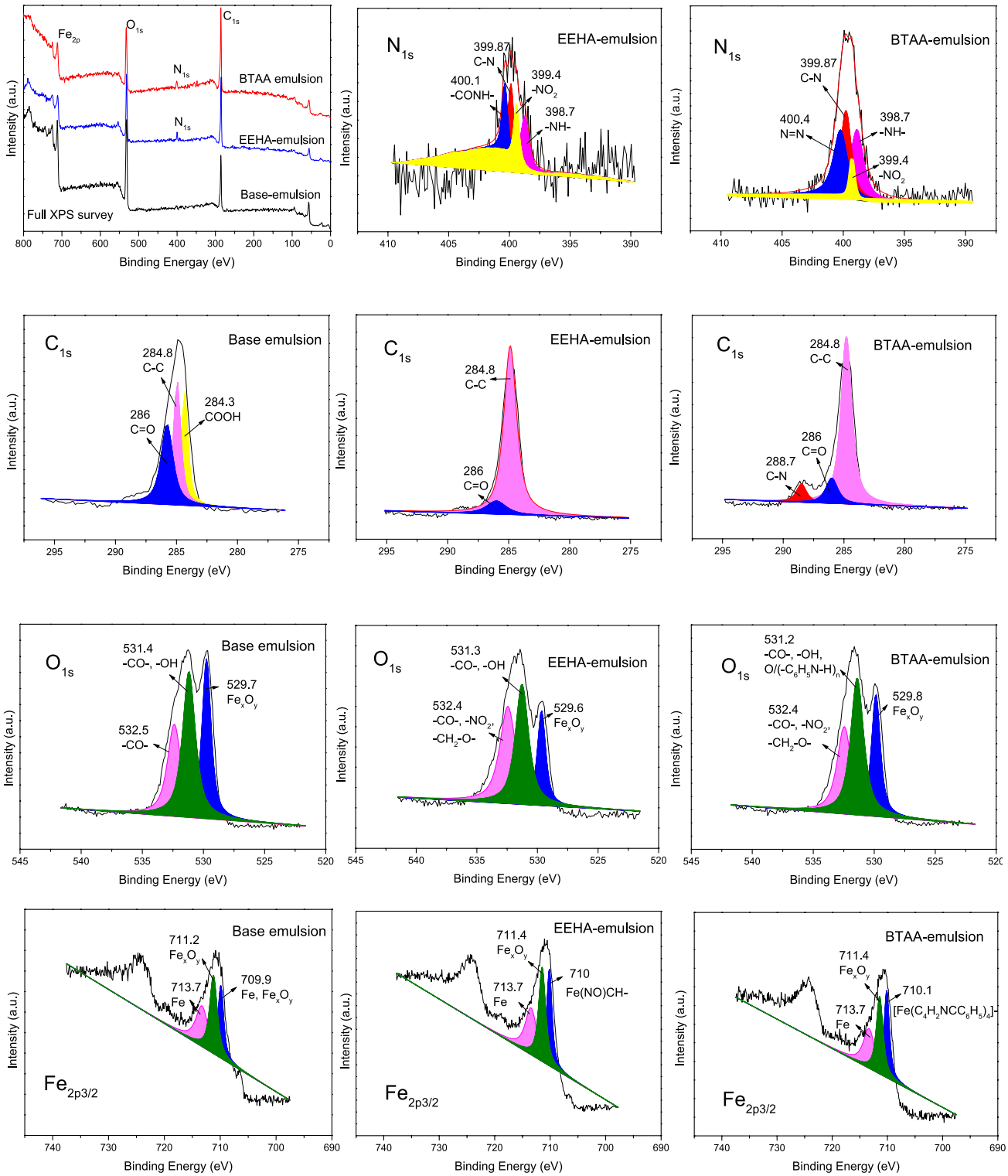

Fig. 10 XPS wide scan and N1s, C1s, O1s, and Fe2p spectra of worn surfaces after lubricating by the base, EEHA- and BTAA-emulsion (velocity 60 mm/s, load 3 N)

BTAA-tribofilm, it can be inferred that tribochemical reactions occurred between additives or between iron atoms and additive molecules during the friction process.

XPS results reveal that during the friction process, additive molecules can be firstly deposited on the rubbing surfaces, and then complex tribochemical reactions occurred

between additive molecules and the steel surface to produce a protective film containing Fe_2O_3, N-containing organics, and Fe–N complexes. In addition, XPS results imply that BTAA molecules were less likely to be destroyed than EEHA molecules. C–N and N=N structures were detected on the BTAA-tribofilm, which may be attributed to the residual benzotriazole ring, and may also be the reason why the BTAA-emulsion showed better tribological properties than the EEHA-emulsion under the corresponding test conditions.

3.3.5 XANES

X-ray absorption near-edge structure (XANES) is a non-destructive technology that can chemically characterize surfaces on the nanoscale. XANES spectroscopy utilizes high-energy X-ray photons from a high-flux synchrotron radiation source, so it is a powerful tool to help characterize thin films and is considered to be a fingerprint of thin-film chemistry [32]. Combining the two modes of total electron yield (TEY) and fluorescence yield (FY) in XANES, the outermost surface (5 nm) and bulk (50 nm) chemical composition of the tribofilm can be checked [33]. N K-edge X-ray absorption spectra can give detailed information about the chemical state of nitrogen in a film. Since the base emulsion does not contain nitrogen, which has also been confirmed in the XPS study. Therefore, the XANES spectroscopy in this study is mainly used to study the tribochemical differences of two different nitrogen-containing molecules on the iron surface. The specific method was to compare the original molecular spectrum before friction with the spectrum of residual molecular fragments or new products on the tribofilm after friction. The N-XANES spectra of the tribofilms and corresponding peak positions obtained in this work are shown in Fig. 11 and Table 5, respectively, untreated additives were also investigated for comparison.

Figure 11 shows that, for all EEHA related samples, absorption peaks at around 406.6 eV and 410 eV are observed, which should be attributed to the σ* state of nitrogen [34]. Compared with the untreated EEHA sample, the spectral peak intensity of the EEHA-tribofilm in both FY and TEY modes is reduced, and this change may be related to the rupture of the C–N bond. However, all the BTAA related samples showed spectral features in the region of 397–402 eV and a bigger peak at 405–415 eV, which corresponded to transitions of the N_{1s}-π* and N_{1s}-σ* type, respectively [34]. In addition, some differences can be found in the absorption peaks of the BTAA-tribofilm in the TEY and FY modes. Unlike the less obvious π* peak in TEY spectra of BTAA-tribofilm, the π* resonance in FY mode is noticeably composed of a combination of three components at 398.4, 399.8, and 400.6 eV. According to literature data, these three components might be attributed to nitrogen

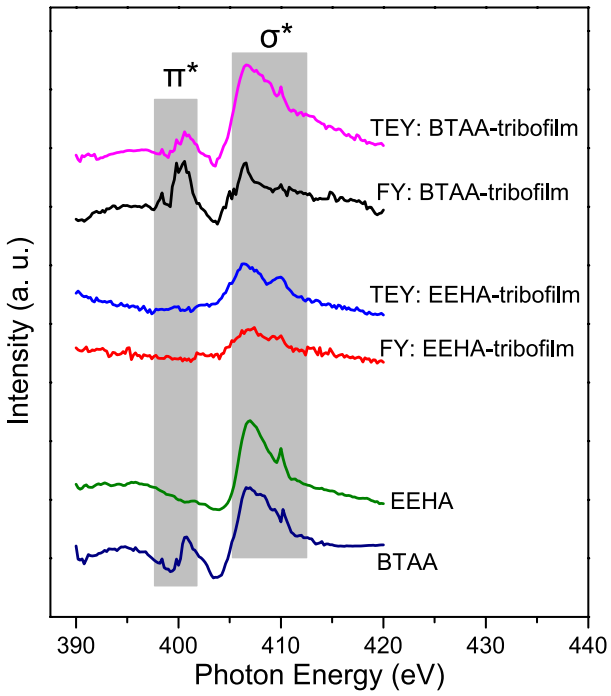

Fig. 11 N K-edge XANES spectra of untreated additives, and tribofilms measured in the TEY and FY modes (velocity 60 mm/s, load 3 N)

Table 5 Peak positions of the N K-edge spectra (TEY and FY) generated from additives and tribofilms

	N K-edge (eV)				
	π*			σ*	
Sample					
TEY: BTAA-tribofilm	398.6	399.8	400.6	406.6	410
FY: BTAA-tribofilm	398.4	399.8	400.6	406.6	410
TEY: EEHA-tribofilm	–	–	–	406.4	410
FY: EEHA-tribofilm	–	–	–	406.8	410
Compounds					
EEHA				406.8	410
BTAA	398.4	399.8	400.6	406.6	410.2

in different structural states, such as pyrrole, cyanide, or graphite-like structures [35]. In addition, the intensity ratio of peak π* to peak σ* in FY mode of BTAA-tribofilm is bigger than that in TEY mode. This indicates that the bottom layer of BTAA-tribofilm mainly contains benzotriazole or other π* state nitrogen, while non- or less-reacted BTAA molecules are the main ingredients at the upper layer of the BTAA-tribofilm.

Overall, N K-edge XANES spectroscopy provides important information on the interaction of additive and metal surfaces. The XANES analysis shows that the tribofilms

generated from O/W emulsions with different additives are different in terms of chemical composition. EEHA-tribofilm contains σ*–N, corresponding to –N–C–. While BTAA-tribofilm was made up of N-containing compounds in both π* and σ* states. N in state π* was introduced by the benzotriazole ring. In addition, different chemical compositions on the surface and bulk regions of BTAA-tribofilm were also observed, that is, the bottom layer of BTAA-tribofilm is mainly composed of π*–N. The XANES spectra of EEHA-tribofilm and BTAA-tribofilm both inform that the C–N bond in the non-heterocyclic structure of the additive molecule was likely to be broken during the friction process, while the cracking possibility of C–N and N=N bonds in the aromatic ring was much less. Since the composition of tribofilm is related to the different tribological properties, XANES analysis gives a good indication of the possible reasons for the different tribological properties of BTAA and EEHA additives.

4 Tribochemical Mechanism

Understanding the mechanisms of tribofilm formation is essential to understanding how it reduces friction and wear. It is hypothesized that the tribological effect of lubricant additives was due to their polar groups that can help additive form ordered adsorbed layers on the sliding metallic surfaces, and further changed into tribochemical films. For N-containing additives used in this work, the lone pair electrons of nitrogen and oxygen atoms in additives can be complexed with the empty orbit of metal iron according to the coordination chemistry theory, and can also be combined with the positive charge of the metal surface to form a stable adsorption film. Furthermore, under boundary friction conditions, mechanical shearing and other reaction-inducing effects, including friction heat, excited electrons, and exposure of high-energy fresh metal surfaces, may cause the adsorbed additives to decompose and react with metal iron, resulting in a tribochemical reaction film. Therefore, the tribofilm is composed of an outer adsorption layer and an inner reaction layer. During the rubbing process, the outer layer could protect the inner layer from being quickly rubbed away.

Based on the worn surface analysis, the difference in the tribological properties between EEHA and BTAA should be ascribed to the difference in tribofilm's structure and change mechanisms on rubbing surfaces. Due to the amphiphilic nature of the molecular structure of EEHA and BTAA, they may exist in the water phase and the water–oil interface in the oil-in-water emulsion. The possible adsorption states and changes of oil, EEHA, and BTAA molecules on metal surfaces during the friction process can be depicted schematically in Fig. 12. The red dashed line in Fig. 12 represents possible bond breakage, and the blue dashed line represents possible π–π stacking and hydrogen bond. It should be noted that the amplified molecular models do not represent the actual proportion.

The molecular structure is a root cause of the difference in the tribological properties between different additives. For the used EEHA and BTAA compounds in this study, the adsorption may occur by coordination through the lone pair electrons of nitrogen and oxygen atoms with iron atoms. Specifically, because of its high nitrogen content, EEHA is likely to be more easily adsorbed to the tribo surface than rapeseed oil. Compared with EEHA, the BTAA molecule was provided with relatively bigger adsorption advantages for the existence of an aromatic ring in its structure. When the BTAA molecule approaches the metal surface, the large π-conjugated electrons on the molecule enter the empty d orbital of Fe, and the anti-π orbital can accept the electrons in the d orbital of Fe to form a feedback bond, thereby forming stable chemical adsorption which will extend the retention time of additive molecules on the metal surface. In this study, the BTAA sample resulted in a smaller COF and wear rate under 3 N loading conditions, which also confirmed this speculation to a certain extent.

The influence of load on the tribological performance is mainly reflected in its influence on the existing state of additive molecules on the metal surface. During the friction process of O/W emulsions as lubricants, because EEHA and BTAA molecules contain multiple hydrophilic functional groups, and the extension of hydrophilic chains in polar water leads to a high probability that the additive molecules adsorbed on the metal surface will be cross-linked by hydrogen bonds, and eventually form a network structure similar to a molecular pad. Under the low load of 1 N, oil and additive molecules are most likely to adsorb perpendicular to the metal surface to achieve the maximum adsorption capacity. However, under high load friction conditions, more additive molecules tended to be adsorbed on the metal surface in a flat state. In addition, the load will also affect the removal rate of the molecules adsorbed on the friction surface and the tribochemical reaction rate. Generally, the load is proportional to these two rates.

When considering the changes of molecules during the friction process, the tribochemical reaction should start with the bond breaking of the additive molecules. From the dissociation energy point of view, the N–X bonds could be easier broken down at the interface since they have lower dissociation energies than some C–C bonds [36]. Specifically, for EEHA additive, after EEHA molecules adsorb on the metal surface by the lone pair electrons of nitrogen and oxygen atoms in the molecule, the molecular structure of EEHA will be gradually destroyed because of the repeated friction process. Since N–X is easier to be fractured, the cleavage of EEHA molecules may start from N–X, releasing many

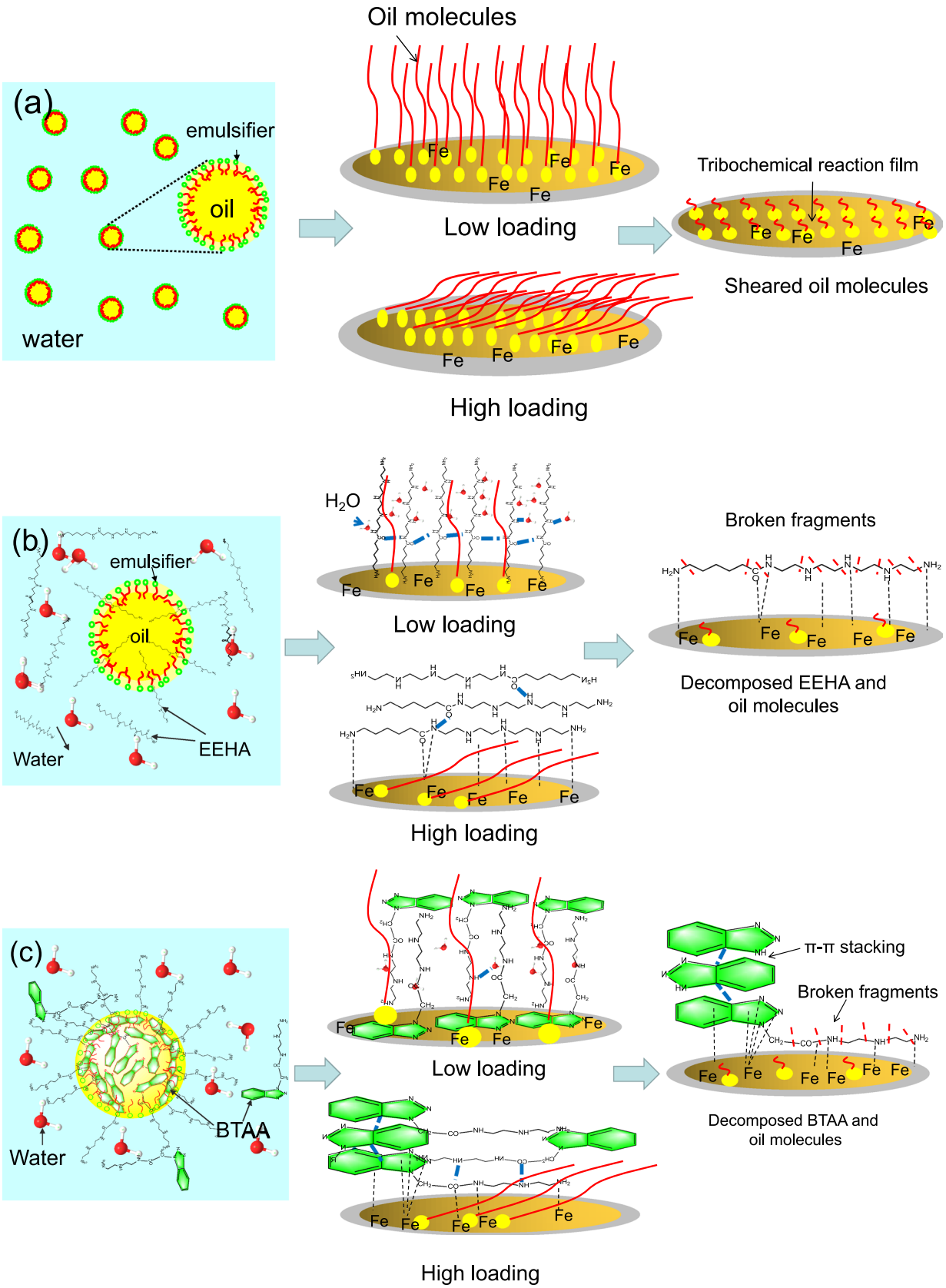

Fig. 12 Possible tribological mechanism of **a** base, **b** EEHA-, and **c** BTAA-emulsion under low and high loading conditions during the friction process

small fragments. This hypothesis can be proved from the reduction of σ* absorption peak in N-XANES. The special feature of the BTAA additive lies in its benzotriazole ring structure, aryl groups in BTAA molecules are more difficult to be cracked [37], therefore, most of the aromatic rings will remain intact and form π–π stacks which can be strongly adhered on the metal surface, instead of being destroyed and releasing small molecular fragments that can be easily removed during the friction process. This conjecture can also be confirmed from the XANES spectra. Moreover, the benzotriazole ring can form π–π stacks, and the formed π–π stacking structure not only increase the thickness of the BTAA-tribofilm but also may decrease the shear strength of lubricating film for the Van der Waals force between benzotriazole molecular layers. Thus, the wear and friction between the contact surfaces were effectively reduced. This explains reasonably why BTAA was a better lubricating additive than EEHA under 3 N loading conditions.

Table 6 presents a summary of COF and wear rates related to 1 N and 3 N conditions. Combining the tribological experimental results in Table 6 and the possible mechanism predicted in Fig. 12, the COFs and wear rates under 1 N and 3 N loads are sorted and summarized in Fig. 13, to more clearly analyze the influence mechanism of molecular structure on tribological performance. It can be seen from Fig. 13a that under the 1 N working condition, point A corresponding to the base emulsion shows the smallest COF, indicating that the long-chain alkyl chain was not sheared or removed under 1 N loading. Therefore, the formed "alkyl molecular brush" exerted the weak interaction force between alkyl chains and achieved the minimum shear force, that is, the minimum COF among the three test samples. For EEHA- and BTAA-emulsion lubrication, additives and oil molecules will be competitively adsorbed on the metal surface, and due to the high nitrogen content of additive molecules, hydrogen bonds can be formed between the adsorbed additive molecules. The water molecules in the emulsion may also be involved in the formation of hydrogen bonds. A large number of hydrogen bonds between two opposite friction surfaces will lead to a big adhesion force and a high COF. Compared with BTAA, the molecular structure of EEHA determines its potential to form more hydrogen bonds. This partially explains why the COF corresponding to EEHA-emulsion is larger than that of BTAA-emulsion under 1 N loading. However, the smallest wear rate is at point B corresponding to EEHA-emulsion. This may be attributed to the amino-functional groups in the EEHA molecule. On the one hand, the amino group acts as an alkaline, thus the metal corrosion caused by the base emulsion can be reduced. On the other hand, its chemical activity is higher than that of benzotriazole, which may produce a relatively effective tribochemical reaction film.

Table 6 Summary of average COFs and wear rates for the three emulsions (velocity 60 mm/s)

Sample	Average COF		Wear rate (10^{-7} $mm^3 \cdot N^{-1} \cdot m^{-1}$)	
	1 N	3 N	1 N	3 N
Base emulsion	0.121	0.140	18.60	29.98
EEHA-emulsion	0.133	0.135	8.72	23.12
BTAA-emulsion	0.128	0.125	16.49	20.11

Due to the high nitrogen content of EEHA and BTAA molecules, their good adsorption ability to the metal surface was fully manifested under high load friction conditions. Figure 13b shows that oil molecules can be easily removed during the 3 N friction process for their low adsorption characteristics to the metal surface. Therefore, base emulsion exhibited the greatest COF and the maximum wear rate under the 3 N loading conditions. The smallest COF and wear rate were produced by BTAA-emulsion under 3 N working conditions, which indicates that high load is beneficial to the tribological effect of BTAA molecules. The possible reason could be that under high loading, BTAA molecules cannot easy to be destroyed, they can remain on the metal surface for a longer time, and form a better adsorption film or tribochemical reaction film than EEHA additive. Considering the low chemical reaction activity of the benzotriazole ring, the probability of forming an excellent adsorption film is greater, and this adsorption film might be a kind of π–π stacking. This π–π stacking effectively compensates for the low chemical reactivity of the benzotriazole ring and results in better tribological properties than EEHA-emulsion.

After the above analysis, the tribological properties and possible mechanisms of several main functional groups involved in the rubbing process in this study can be further refined. The results are summarized in Table 7. The smiley face pattern represents favorable. It can be seen from Table 7 that the benzotriazole ring can simultaneously reduce COF and wear rate under high load friction conditions. Raman, EDS, XPS, and XANES analysis indicate that the BTAA additive, which contains benzotriazole ring in its molecular structure, probably formed π–π stacking on the rubbing surface, thus resulting in good tribological properties.

Figure 14 shows the inferred model of the self-lubricating friction film formed by the BTAA-emulsion. The oil solubility and metal adsorption characteristics of BTAA molecules make the most of the BTAA can be adsorbed on the metal surface during the friction process, and some unadsorbed sites were filled with oil molecules, resulting in fewer exposed metal sites, which means that the metal surface is affected by better protection. Hydrophobic protective film formed by mixing oil molecules and BTAA molecules can effectively hinder the transfer of charges

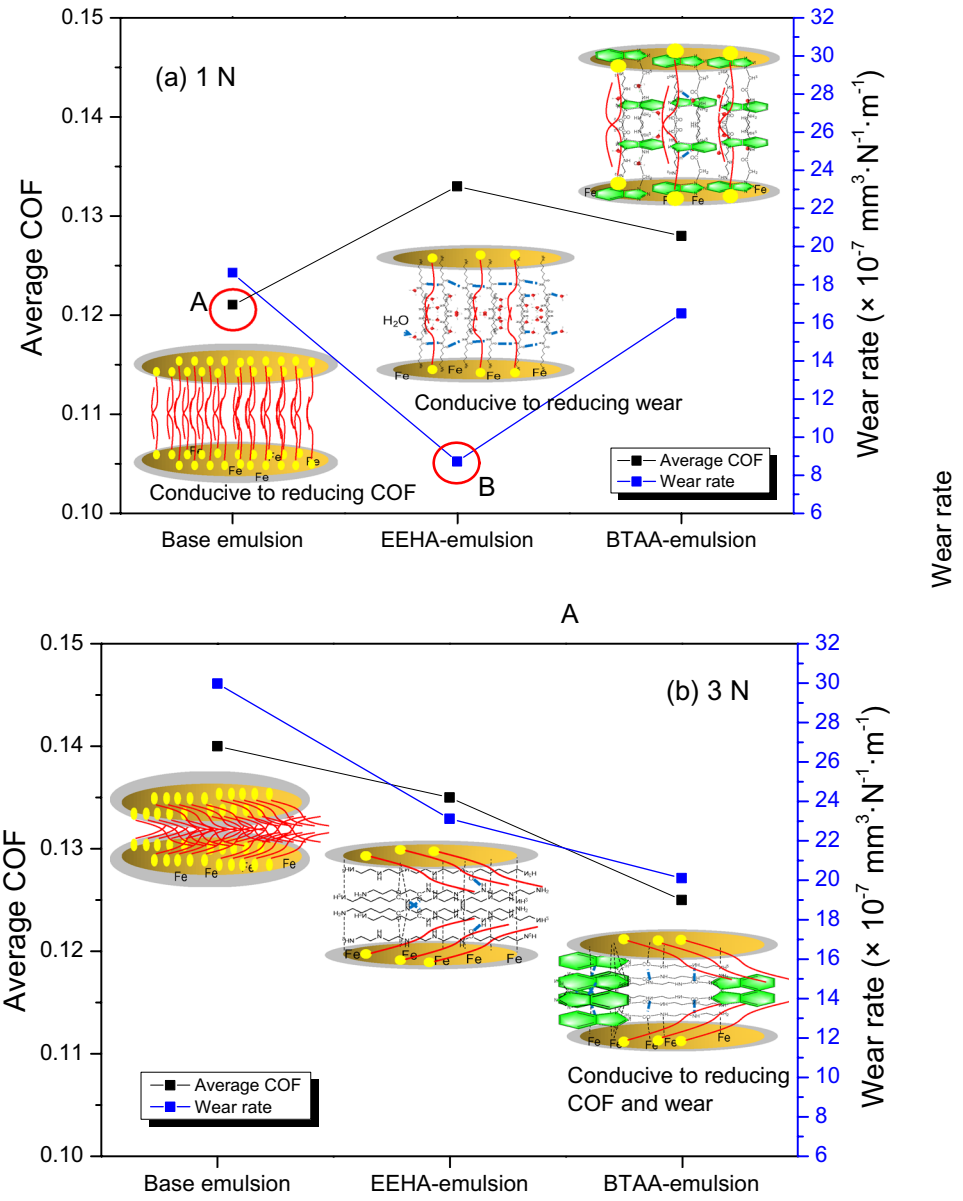

Fig. 13 The COFs, wear rates, and possible friction models of three different emulsions under 1 N and 3 N loading conditions (velocity 60 mm/s)

Table 7 Summary of advantages and possible mechanisms of main frictional components

	Feature	Low load (1 N)		High load (3 N)		Possible mechanisms
		COF	Wear rate	COF	Wear rate	
Rapeseed oil	Long alkyl chain	😃				Weak force
EEHA	Amino ($-NH_2$)		😃			Reduce corrosion wear
BTAA	Benzotriazole ring			😃	😃	Π–π stacking

or substances related to the oxidation reaction, thereby inhibiting interfacial corrosion. In the later stage of friction, oil molecules and BTAA molecules were damaged by shearing force, and benzotriazole heterocycles that were not easily decomposed may form π–π stacks. Although the chemical reaction activity of the benzotriazole functional group is relatively low, the π–π accumulation film formed by the benzotriazole functional group may effectively offset this defect. Therefore, in terms of the overall effect, the BTAA additive shows better friction-reducing

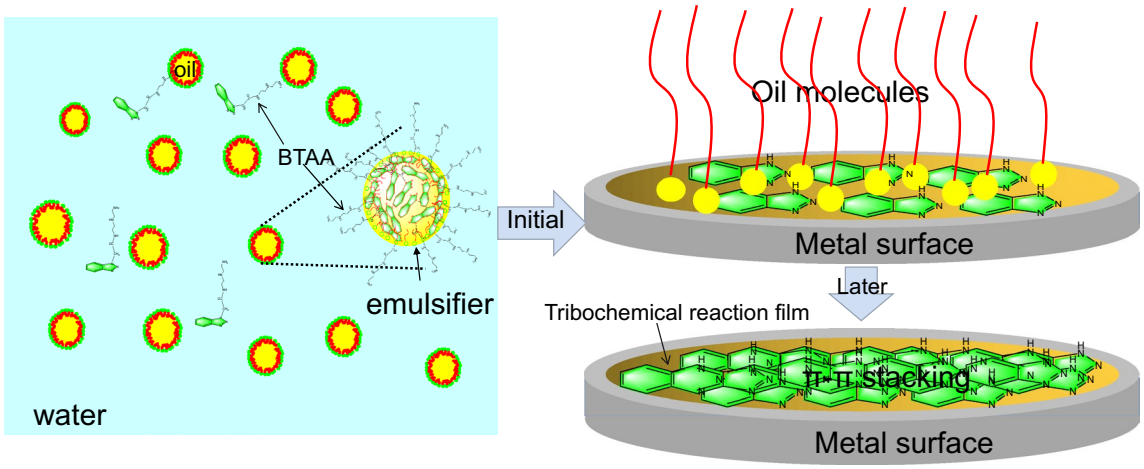

Fig. 14 The conceived model of the BTAA-emulsion forms a self-assembled lubricating film under high loading

and anti-wear performance than EEHA under a high load of 3 N in this work.

In summary, EEHA and BTAA additives might be adsorbed to the metal surface faster than the "plate-out" of oil droplets. This resulted in the adsorption film formed by the additive-containing emulsion may be composed of a large number of additive molecules and a small number of oil molecules. Based on the worn surface analysis and above mechanism speculation, it can be inferred that as-synthesized amide additives in O/W were decomposed during the sliding process. Under appropriate conditions, the decomposed products will react with the metal surface, therewith giving rise to the protective film containing Fe_2O_3, nitro compounds, and Fe–N complexes. The surface protective film can prevent direct contact between the sliding surfaces of the friction pair, thereby reducing friction or wear. The interesting result was that benzotriazole rings in BTAA molecules might form a self-assembled adsorption film on the rubbing surface through π–π stacking. The π–π stacking species is a more compact barrier layer, which could lead to a better tribological effect, and a high load is more conducive to its formation. Tribological results showed that it can effectively make up for the lack of reactivity of benzotriazole heterocycle during the friction process, and lead to the best friction-reducing and anti-wear properties of BTAA additive under high loading conditions.

5 Conclusions

In this paper, two water-soluble nitrogen-containing additives without sulfur and phosphorus were added to the oil-in-water emulsion to study the influence of different forms of nitrogen-containing functional groups (amino group and benzotriazole rings) on the tribological properties of the oil-in-water emulsion. In the context of coefficient of friction (COF), wear rate, and worn surface characterization, the effectiveness of additives to reduce friction and wear under boundary lubrication conditions was investigated. Based on the presented results and discussion, the following conclusions can be drawn from this research.

(1) The synthesized products were characterized by infrared spectroscopy (IR), nuclear magnetic resonance spectroscopy (NMR, ^{1}H and ^{13}C), and elemental analysis. The results confirmed the successful preparation of the two N-containing additives, EEHA and BTAA.
(2) COFs indicate that N-containing additives might adsorb faster onto the metal surface than oil molecules, which would affect the formation of the “plate-out” oil film and hence result in the increased COF under 1 N loading conditions when compared with base emulsion. However, the additives exerted friction-reducing performance under 3 N loading conditions, and BTAA-emulsion appeared to be the most effective one with the lowest COF, which is 10.7% lower than that of base emulsion, 7.4% lower than that of EEHA-emulsion.
(3) Both EEHA and BTAA showed anti-wear properties in all experimental tests in this study. This could be because both of them contain amino functional groups, and the alkaline nature of amino groups helps to reduce corrosion wear.
(4) The smallest roughness result of the worn surfaces corresponding to BTAA-emulsion lubrication confirms that the BTAA-emulsion performed better than the base and EEHA-emulsion in preventing the tribopair contact and wear under the 3 N friction condition.

(5) The nanomechanical results reveal that the EEHA- and BTAA-tribofilm behaved as a soft protective layer on the steel substrate, and BTAA-tribofilm shows the most prominent softness.
(6) The Raman spectra of the worn surfaces lubricated with different emulsions confirm the presence of benzotriazole rings in the BTAA-tribofilm.
(7) EDS results show that the formed tribofilms are mainly composed of high-carbon-containing substances, and the increase in load may accumulate more π–π deposits. This may be because high loading can reduce the spacing of aromatic rings and enhance the conjugation of π electrons. Based on the molecular structure of BTAA, it can be speculated that BTAA molecules were sheared and damaged during friction, and the high-carbon substances were likely to be formed by π–π stacking of benzotriazole rings.
(8) XPS analysis indicates that tribochemical reactions occurred between the lubricant and the metal surfaces during the friction process. Protective films consisting of Fe_2O_3, N-containing compounds, and Fe–N complexes were formed on rubbed steel surfaces. The C=N bond was additionally found in the BTAA-tribofilm, indicating that there may be tribochemical products containing benzotriazole ring structures.
(9) N-XANES analysis shows that the tribofilms generated by O/W emulsions containing different additives were different in chemical composition. EEHA-tribofilm contained σ*–N, while BTAA-tribofilm was made up of N-containing compounds in both π* and σ* states. In addition, different chemical compositions of the surface and the bulk region of BTAA-tribofilm were also observed, that is, the bottom layer of BTAA-tribofilm mainly existed in the π* state. XANES analysis informed that the C–N bond in the non-heterocyclic structure of the additive molecule was likely to be cleaved during the friction process, while the possibility of C–N bond and N=N bond breaking in the aromatic ring structure was much less.
(10) Tribological molecular mechanism analysis shows that the superior tribological properties of the BTAA under 3 N conditions should be ascribed to the benzotriazole ring in molecular structure. This kind of aromatic ring is not easy to decompose and may form π–π stacking during the friction process. This π–π stacking effectively compensates for the low chemical reaction activity of the benzotriazole ring and leads to the best tribological properties of BTAA-emulsion among the three tested emulsions.

Acknowledgements The authors would like to thank the financial support from Shanghai University of Engineering Science and the National Natural Science Foundation of China (51965020). The authors are also grateful to the Beijing synchrotron radiation facility and Shanghai Jiao tong University for their technical support.

Declarations

Conflict of interest The authors declare that they have no known competing financial interests or personal relationships that could have appeared to influence the work reported in this paper.

Ethical Approval We confirm that this manuscript is the authors' original work and has not been published nor has it been submitted simultaneously elsewhere. All authors have checked the manuscript and agreed to the submission.

References

1. Meng, Y.G., Xu, J., Jin, Z.M., Prakash, B., Hu, Y.Z.: A review of recent advances in tribology. Friction **8**, 221–300 (2021). https://doi.org/10.1007/s40544-020-0367-2
2. Peng, Y.X., Wang, G.F., Zhu, Z.C., Chang, X.D., Lu, H., Tang, W., Jiang, F., Chen, G.A.: Effect of low temperature on tribological characteristics and wear mechanism of wire rope. Tribol. Int. **164**, 107231 (2021). https://doi.org/10.1016/J.TRIBOINT.2021.107231
3. Tian, X., Song, N.N., Yang, G.B., Zhou, C.H., Zhang, S.M., Zhang, P.Y.: Organic-sulfonate functionalized graphene as a high temperature lubricant for efficient antifriction and antiwear in water based drilling fluid. Tribol. Lett. **70**, 32 (2022). https://doi.org/10.1007/S11249-022-01575-6
4. Khanmohammadi, H., Wijanarko, W., Espallargas, N.: Ionic liquids as additives in water-based lubricants: from surface adsorption to tribofilm formation. Tribol. Lett. **68**, 130 (2020). https://doi.org/10.1007/s11249-020-01377-8
5. Xue, S.Q., Cen, Y.M., Yang, H.M., Zeng, X.Q.: The enhanced lubrication of water-based cutting fluid by functionalized GO. Tribol. Lett. **68**, 19–37 (2020). https://doi.org/10.1007/s11249-020-01324-7
6. Reddyhoff, T., Ku, I.S.Y., Holmes, A.S., Spikes, H.A.: Friction modifier behaviour in lubricated MEMS devices. Tribol. Lett. **41**, 239–246 (2011). https://doi.org/10.1007/s11249-010-9704-3
7. González, R., Ramos, D., Blanco, D., Fernández-González, A., Viesca, J.L., Hadfield, M., Battez, A.H.: Tribological performance of tributylmethylammonium bis(trifluoromethylsulfonyl)amide as neat lubricant and as an additive in a polar oil. Friction **7**, 282–288 (2019). https://doi.org/10.1007/s40544-018-0231-9
8. Faujdar, E., Negi, H., Bhonsle, A., Atray, N., Singh, R.K.: Efficiency of dodecenylsuccinic amide of n-phenyl-p-phenylenediammine as novel multifunctional lubricant additive for deposit control and lubricity. J. Surfactants Deterg. **24**, 173–184 (2020). https://doi.org/10.1002/JSDE.12456
9. Yan, J.C., Zeng, X.Q., Ren, T.H., van der Heide, E.: Boundary lubrication of stainless steel and CoCrMo alloy based on phosphorous and boron compounds in oil-in-water emulsion. Appl. Surf. Sci. **315**, 415–424 (2014). https://doi.org/10.1016/j.apsusc.2014.07.160
10. Zheng, G.L., Ding, T.M., Zheng, L., Ren, T.H.: The lubrication effectiveness of dialkylpentasulfide in synthetic ester and its emulsion. Tribol. Int. **122**, 76–83 (2018). https://doi.org/10.1016/j.triboint.2018.02.041
11. Kavita, Kuntail, J., Verma, D.K., Kumar, B., Singh, A.K., Shukla, N., Sinha, I., Rastogi, R.B.: Theoretical and experimental studies

of pyranopyrazoles and theirtribological compatibility with a borate ester. Colloid Surf. A **606**, 125497 (2020). https://doi.org/10.1016/j.colsurfa.2020.125497
12. Lei, G.: Crystal structure and luminescent property of the magnesium complex $[Mg(phen)(H_2O)_4]\cdot[3,5\text{-}(SO_3)H_2cat]\cdot 2.5(phen)\cdot 3H_2O$. Synth. React. Inorg. Met. **46**, 1–5 (2016). https://doi.org/10.1080/15533174.2013.865231
13. Hsien, W.L.Y.: Towards Green Lubrication in Machining. Springer, Singapore (2015)
14. Lee, S., Heeb, R., Venkataraman, N.V., Spence, N.D.: Macroscopic tribological testingof alkanethiol self-assembled monolayers (SAMs): pin-on-disk tribometry withelastomeric sliding contacts. Tribol. Lett. **28**, 229–239 (2007). https://doi.org/10.1007/s11249-007-9266-1
15. Wu, Y.L., Sun, T., He, Z.Y., Zeng, X.Q., Ren, T.H., de Vries, E., van der Heide, E.: Study on the relationship between the tribological properties and oxidation degree of graphene derivatives in O/W emulsion. Tribol. Int. **157**, 106875 (2021). https://doi.org/10.1016/j.triboint.2021.106875
16. Liang, X.P., Yang, X.G., Wu, J.Q., Tu, Z.B., Wang, Y., Yuan, Y.: Effect of alcohol additives on the plate out oil film in cold rolling and its molecular dynamics simulations. Tribol. Trans. **62**, 504–511 (2019). https://doi.org/10.1080/10402004.2019.1581312
17. Choudhry, J., Almqvist, A., Larsson, R.: A Multi-scale Contact Temperature Model for Dry Sliding Rough Surfaces. TRIBOL LETT. **69**, 128 (2021). https://doi.org/10.1007/s11249-021-01504-z
18. Song, J.P., Liu, S.W., Rafiq, A., Gao, J.J., Lv, M.: Tribological behaviour of TiB2-HfC ceramic tool material under dry sliding condition. Ceram. Int. **46**, 20320–20327 (2020). https://doi.org/10.1016/j.ceramint.2020.05.120
19. Chen, Z.H., Bao, C.G., Wu, G.Q., Jian, Y.X., Huang, Z.F., Ma, H.Q.: Effects of YAl2 reinforced particles on the tribological properties of LA143 alloy under dry sliding condition. Wear **438–439**, 203077 (2019). https://doi.org/10.1016/j.wear.2019.203077
20. Liang, Y.N., Gao, D.R., Zhao, J.H.: Tribological properties of friction pair between 316L stainless steel and CF/PEEK with nonsmooth surface under seawater lubrication. Tribol. Trans. **63**, 658–671 (2020). https://doi.org/10.1080/10402004.2020.1734704
21. Ramesh, A., Melkote, S.N.: Modeling of white layer formationder thermally dominant conditions in orthogonal machining of hardened AISI 52100 steel. INT J MACH TOOL MANU. **48**, 402–414 (2008). https://doi.org/10.1016/j.ijmachtools.2007.09.007
22. Wu, Y.L., Zeng, X.Q., Ren, T.H., de Vries, E., van der Heide, E.: The emulsifying and tribological properties of modified graphene oxide in oil-in-water emulsion. Tribol. Int. **105**, 304–316 (2017). https://doi.org/10.1016/j.triboint.2016.10.024
23. Kontomaris, S.V., Malamou, A.: Hertz model or Oliver & Pharr analysis? Tutorial regarding AFM nanoindentation experiments on biological samples. MATER RES EXPRESS. **7**, 033001 (2020). https://doi.org/10.1088/2053-1591/ab79ce
24. Stewart, K.L., Zhang, J., Li, S.T., Carter, P.W., Gewirth, A.A.: Anion effects on Cu-benzotriazole film formation: implications for CMP. J. Electrochem. Soc. **154**, D57–D63 (2006). https://doi.org/10.1149/1.2393013
25. Chang, Y., Yang, Z.G.: Additive fabrication of conductive patterns by a template transfer process based on benzotriazole adsorption as a separation layer. ACS Appl. Mater. Interfaces **8**, 14211–14219 (2016). https://doi.org/10.1021/acsami.6b00499
26. Andrikopoulos, P.C., McCarney, K.M., Armstrong, D.R., Littleford, R.E., Graham, D., Smith, W.E.: A density functional theory and resonance Raman study of a benzotriazole dye used in surface enhanced resonance Raman scattering. J. Mol. Struct. **789**, 59–70 (2005). https://doi.org/10.1016/j.molstruc.2005.12.021
27. Guo, X.L., Hurley, B., Yang, F., Buchheit, R.: A novel organic conversion coating based on N-benzoyl-N-phenylhydroxylamine chemistry for the corrosion protection of AA2024-T3. Electrochim. Acta **246**, 197–207 (2017). https://doi.org/10.1016/j.electacta.2017.06.049
28. Lahouij, I., Gould, B., Demas, N., Greco, A., Chen, Z., Cooper, G.D., Jackson, A., Carpick Robert, W.: Inhibition of micropitting by tribofilm-forming ZrO_2 nanocrystal lubricant additives: a micro-pitting rig and transmission electron microscope study. Tribol. Lett. **70**, 13 (2022). https://doi.org/10.1007/S11249-021-01555-2
29. Gu, W.C., Qi, S.S., He, W.H., Chu, K., Lu, Z.B., Zhang, G.G.: Different tribological behaviors in multilayer 2D graphene and 3D graphene foam modified DLC/H-DLC film in moist air. Tribol. Lett. **70**, 16 (2022). https://doi.org/10.1007/S11249-021-01556-1
30. Naumkin, A.V., Kraut-Vass, A., Gaarenstroom, S.W., Powell. C.J.: NIST X-ray photoelectron spectroscopy database. NIST Standard Reference Database 20, Version 4.1. https://srdata.nist.gov/xps/Default.aspx. Accessed 17 Mar 2022
31. Yang, G.B., Zhang, J.F., Zhang, S.M., Yu, L.G., Zhang, P.Y., Zhu, B.L.: Preparation of triazine derivatives and evaluation of their tribological properties as lubricant additives in poly-alpha olefin. Tribol. Int. **62**, 163–170 (2013). https://doi.org/10.1016/j.triboint.2013.02.024
32. Adam, A., Charlotte, B., Josef, B., Serhiy, B., Marcella, F., Nicole, D.: Engine oils in the field: a comprehensive tribological assessment of engine oil degradation in a passenger car. Tribol. Lett. **70**, 28 (2022). https://doi.org/10.1007/S11249-022-01566-7
33. Cutler, J.N., Sanders, J.H., Zabinski, J.S., John, P.J., McCutchen, J.R., Kasten, L.S., Tan, K.H.: Surface chemistry of new lubrication systems for high-speed spacecraft bearings. Tribol. Lett. **8**, 17–23 (2000). https://doi.org/10.1023/A:1019166630462
34. Chagas, M.R.M., Quirino, W.G., Neto, A.M.J.C., Sousa, E.A.D., Cremona, M., Rocco, M.L.M., Mota, G.V.S.: Degradation of the N, N′-bis-(1-naphthyl)-N, N′-diphenyl-1,1′-biphenyl-4,4′-diamine by photon irradiation. Thin Solid Films **517**, 4461–4463 (2009). https://doi.org/10.1016/j.tsf.2009.01.083
35. Svintsitskiy, D.A., Kibis, L.S., Smirnov, D.A., Suboch, A.N., Stonkus, O.A., Podyacheva, O.Y., Boronin, A.I., Ismagilov, Z.R.: Spectroscopic study of nitrogen distribution in N-doped carbon nanotubes and nanofibers synthesized by catalytic ethylene-ammonia decomposition. Appl. Surf. Sci. **435**, 1273–1284 (2018). https://doi.org/10.1016/j.apsusc.2017.11.244
36. Zhao, H.Y., Neville, A., Morina, A., Vickerman, R., Durham, J.: Improved anti-shudder performance of ATFs—influence of a new friction modifier and surface chemistry. TRIBOL INT. **46**, 62–72 (2011). https://doi.org/10.1016/j.triboint.2011.06.012
37. Mangolini, F., Rossi, A., Spencer, N.D.: Influence of metallic and oxidized iron/steel on the reactivity of triphenyl phosphorothionate in oil solution. Tribol. Int. **44**, 670–683 (2010). https://doi.org/10.1016/j.triboint.2010.02.009